Energy bands of a (111) iron thin film*

D. G. Dempsey, Leonard Kleinman, and Ed Caruthers
Department of Physics, University of Texas, Austin, Texas 78712
(Received 22 December 1975)

We have performed a tight-binding calculation of the energy bands of a 40-layer (111) ferromagnetic iron thin film. The matrix parameters were obtained by fitting a bulk calculation of Tawil and Callaway with the diagonal matrix elements of the layers near the surface shifted to obtain surface charge neutrality. The energy bands were calculated at 61 points in the irreducible (1/12) two-dimensional Brillouin zone. The planar and total densities of states are determined and compared to previous results. The differences between the apparent surface potential on this face of iron compared to the (100) and (110) faces are examined and discussed. Correlations between the energy-band structure and the planar densities of states are examined.

I. CALCULATIONAL TECHNIQUES AND THE DENSITY OF STATES

In previous papers we reported calculations of the energy bands and densities of states of 41-layer (100) (Ref. 1) and 29-layer (110) (Ref. 2) thin films of ferromagnetic iron. Because the bcc (100), (110), and (111) interplanar spacings are $\frac{1}{2}a$, $a/\sqrt{2}$, and $a/2\sqrt{3}$, respectively, a (111) film of the same thickness would contain 71 layers. Due to the low symmetry of (111) films, even with considerably more computational effort, we were limited to a 40-layer film in this calculation. We used the same nine basis functions per atom (one $4s$, three $4p$, and five $3d$) and bulk[3]-derived parameters as for the other faces. However a (111) bcc film possesses neither the two-fold normal rotational axis, which we used in the previous cases to construct real planar Bloch functions, nor the central reflection plane which allowed the Hamiltonian matrix to be reduced by essentially a factor of 2.

The (111) film unit cell is a hexagonal cylinder containing one atom from every plane of the film. There are three types of planes, labeled A, B, and C as in the paper of Caruthers *et al.*,[4] depending on whether the atom is located at the center or alternate corners of the hexagon. If we chose a film with an even number of layers, 40 in our case, and orient the hexagonal unit cell so that the two layers adjacent to the center of the film are B- and C-type planes, the film will have an inversion center. The two-dimensional Brillouin zone (2D BZ) corresponding to this unit cell is a hexagon, rotated 90° with respect to its real space counterpart, having symmetry points and lines as depicted by Caruthers *et al.*[4] If we use our nine Bloch functions per plane as a basis [as we did on the (100) and (110) faces], our Hamiltonian will be a 360×360 matrix and, unless we are at $\bar{\Gamma}$ or $\bar{M}$ (where inversion is a member of the group of $\bar{k}$), this matrix will be complex. Thus, except at $\bar{\Gamma}$ and $\bar{M}$, the film's inversion symmetry can neither be used to reduce the matrix size nor to make it real and the problem becomes computationally unmanageable.

To overcome this difficulty, we combine, at points other than $\bar{\Gamma}$ and $\bar{M}$, functions of $+\bar{k}$ and $-\bar{k}$ to produce a new set of 18 Bloch basis functions per plane which are real and will, therefore, produce a real 720×720 Hamiltonian matrix. Using the inversion symmetry (which is a member of the group of the combined wave vectors $+\bar{k}$ and $-\bar{k}$) this is reduced into two identical real 360×360 matrices. By combining even and odd degenerate eigenfunctions from the two matrices one can regain $+\bar{k}$ and $-\bar{k}$ Bloch functions.

At $\bar{\Gamma}, \bar{K}, \bar{M}$ and along the symmetry lines $\bar{\Sigma}$, $\bar{T}$, and $\bar{T}'$ the size of the matrix is further reduced by using the symmetrized combinations of basis functions listed in Table I. The compatibility relations are listed in Table II.

This Hamiltonian was evaluated separately for the majority and minority spin cases at 61 points[5] in the $\frac{1}{12}$ 2D BZ (576 points in the full 2D BZ). The total and planar densities of states (TDS and PDS) were then calculated in the same way as on the (110) face.[6] The zeroth-neighbor parameters on the planes near the surface were adjusted to produce a charge neutral surface.

On the (100) and (110) surfaces, charge neutrality was obtained by shifting the ss_0, pp_0, and dd_0 parameters on the surface layer by −0.022 Ry. For this face, the Fermi energy (corresponding to 8.00 electrons/atom in the bulk) is at −0.335 Ry as it was on the other faces. With no shift in the surface parameter the surface layer has a deficit of −0.42 electrons/atom with smaller but noticeable deficits on the two layers adjacent to the surface and small surpluses on the preceding layers. When the surface parameters were shifted −0.022 Ry as before, the surface layer had a surplus of 0.19 electrons/atom while the adjacent nineteenth

TABLE I. Symmetrized combinations of basis functions transforming according to the group of the two-dimensional (2D) wave vector at symmetry points and lines. The 2D unit cell is assumed to be scaled and oriented such that one of the nearest neighbors in the plane is at a Cartesian coordinate $(1,0)$ and the normal direction to the plane is z. The basis functions are given by their transforming symmetry (i.e., $z \equiv p_z$). The subscripts 1–4 denote the construction of the function f such that

$$f_1 = \sum_j [f(\vec{r}-\vec{R}_j) \pm f(\vec{r}+\vec{R}_j)] \cos\bar{k}\cdot\bar{R}_j\ , \quad f_2 = \sum_j [f(\vec{r}-\vec{R}_j) \mp f(\vec{r}+\vec{R}_j)] \sin\bar{k}\cdot\bar{R}_j\ ,$$

$$f_3 = \sum_j [f(\vec{r}-\vec{R}_j) \pm f(\vec{r}+\vec{R}_j)] \sin\bar{k}\cdot\bar{R}_j\ , \quad f_4 = \sum_j [f(\vec{r}-\vec{R}_j) \mp f(\vec{r}+\vec{R}_j)] \cos\bar{k}\cdot\bar{R}_j\ .$$

The upper sign applies to s and d functions and the lower sign to p functions. The three-dimensional (3D) vector $\vec{R}$ selects a particular plane and the sum runs over all sites j on that plane. For all $\bar{k}$ except $\bar{\Gamma}$ and $\bar{M}$, the subscripts 1 and 2 may be replaced by 3 and 4, respectively, producing the two-fold degeneracy discussed in the text.

Symmetry	Basis functions
	$\bar{\Gamma} = (0,0)$
$\bar{\Gamma}_1^+$	$s_1,\ z_1,\ (3z^2-r^2)_1$
$\bar{\Gamma}_1^-$	$s_4,\ z_4,\ (3z^2-r^2)_4$
$\bar{\Gamma}_3^{(1)+}$	$y_1,\ yz_1,\ (x^2-y^2)_1$
$\bar{\Gamma}_3^{(2)+}$	$x_1,\ xy_1,\ xz_1$
$\bar{\Gamma}_3^{(1)-}$	$y_4,\ yz_4,\ (x^2-y^2)_4$
$\bar{\Gamma}_3^{(2)-}$	$x_4,\ xy_4,\ xz_4$
	$\bar{M} = (0, 2\pi/\sqrt{3})$
$\bar{M}_1^+$	A: $s_1,\ y_1,\ z_1,\ yz_1,\ (x^2-y^2)_1,\ (3z^2-r^2)_1$
	B: $(\frac{1}{2}s_1 - \frac{1}{2}\sqrt{3}\,s_2)$, $(\frac{1}{2}y_1 - \frac{1}{2}\sqrt{3}\,y_2)$, $(\frac{1}{2}z_1 - \frac{1}{2}\sqrt{3}\,z_2)$, $(\frac{1}{2}yz_1 - \frac{1}{2}\sqrt{3}\,yz_2)$, $[\frac{1}{2}(x^2-y^2)_1 - \frac{1}{2}\sqrt{3}(x^2-y^2)_2]$, $[\frac{1}{2}(3z^2-r^2)_1 - \frac{1}{2}\sqrt{3}\,(3z^2-r^2)_2]$
	C: $(\frac{1}{2}s_1 + \frac{1}{2}\sqrt{3}\,s_2)$, $(\frac{1}{2}y_1 + \frac{1}{2}\sqrt{3}\,y_2)$, $(\frac{1}{2}z_1 + \frac{1}{2}\sqrt{3}\,z_2)$, $(\frac{1}{2}yz_1 + \frac{1}{2}\sqrt{3}\,yz_2)$, $[\frac{1}{2}(x^2-y^2)_1 + \frac{1}{2}\sqrt{3}(x^2-y^2)_2]$, $[\frac{1}{2}(3z^2-r^2)_1 + \frac{1}{2}\sqrt{3}\,(3z^2-r^2)_2]$
$\bar{M}_1^-$	A: $s_4,\ y_4,\ z_4,\ yz_4,\ (x^2-y^2)_4,\ (3z^2-r^2)_4$
	B: $(\frac{1}{2}\sqrt{3}s_3 + \frac{1}{2}s_4)$, $(\frac{1}{2}\sqrt{3}\,y_3 + \frac{1}{2}y_4)$, $(\frac{1}{2}\sqrt{3}\,z_3 + \frac{1}{2}z_4)$, $(\frac{1}{2}\sqrt{3}yz_3 + \frac{1}{2}yz_4)$, $[\frac{1}{2}\sqrt{3}\,(x^2-y^2)_3 + \frac{1}{2}(x^2-y^2)_4]$, $[\frac{1}{2}\sqrt{3}\,(3z^2-r^2)_3 + \frac{1}{2}(3z^2-r^2)_4]$
	C: $(\frac{1}{2}\sqrt{3}\,s_3 - \frac{1}{2}s_4)$, $(\frac{1}{2}\sqrt{3}\,y_3 - \frac{1}{2}y_4)$, $(\frac{1}{2}\sqrt{3}\,z_3 - \frac{1}{2}z_4)$, $(\frac{1}{2}\sqrt{3}yz_3 - \frac{1}{2}yz_4)$, $[\frac{1}{2}\sqrt{3}\,(x^2-y^2)_3 - \frac{1}{2}(x^2-y^2)_4]$, $[\frac{1}{2}\sqrt{3}\,(3z^2-r^2)_3 - \frac{1}{2}(3z^2-r^2)_4]$
$\bar{M}_2^+$	A: $x_1,\ xy_1,\ xz_1$
	B: $(\frac{1}{2}x_1 - \frac{1}{2}\sqrt{3}\,x_2)$, $(\frac{1}{2}xy_1 - \frac{1}{2}\sqrt{3}\,xy_2)$, $(\frac{1}{2}xz_1 - \frac{1}{2}\sqrt{3}\,xz_2)$
	C: $(\frac{1}{2}x_1 + \frac{1}{2}\sqrt{3}\,x_2)$, $(\frac{1}{2}xy_1 + \frac{1}{2}\sqrt{3}\,xy_2)$, $(\frac{1}{2}xz_1 - \frac{1}{2}\sqrt{3}\,xz_2)$
$\bar{M}_2^-$	A: $x_4,\ xy_4,\ xz_4$
	B: $(\frac{1}{2}\sqrt{3}\,x_3 + \frac{1}{2}x_4)$, $(\frac{1}{2}\sqrt{3}\,xy_3 + \frac{1}{2}xy_4)$, $(\frac{1}{2}\sqrt{3}\,xz_3 + \frac{1}{2}xz_4)$
	C $(\frac{1}{2}\sqrt{3}\,x_3 - \frac{1}{2}x_4)$, $(\frac{1}{2}\sqrt{3}\,xy_3 - \frac{1}{2}xy_4)$, $(\frac{1}{2}\sqrt{3}\,xz_3 - \frac{1}{2}xz_4)$
	$\bar{K}(\frac{2}{3}\pi, 2\pi/\sqrt{3})$
$\bar{K}_1^+$	A: $s_1,\ z_1,\ (3z^2-r^2)_1$
	B: $(1/2\sqrt{2})(\sqrt{3}\,x_1 - y_1 + x_2 + \sqrt{3}\,y_2)$, $(1/2\sqrt{2})(\sqrt{3}\,xz_1 - yz_1 + xz_2 + \sqrt{3}\,yz_2)$, $(1/2\sqrt{2})[\sqrt{3}\,xy_1 - (x^2-y^2)_1 + xy_2 + \sqrt{3}\,(x^2-y^2)_2]$
	C: $(1/2\sqrt{2})(\sqrt{3}\,x_1 - y_1 - x_2 - \sqrt{3}\,y_2)$, $(1/2\sqrt{2})(\sqrt{3}\,xz_1 - yz_1 - xz_2 - \sqrt{3}\,yz_2)$, $(1/2\sqrt{2})[\sqrt{3}\,xy_1 - (x^2-y^2)_1 - xy_2 - \sqrt{3}\,(x^2-y^2)_2]$

TABLE I. *(Continued)*

Symmetry	Basis functions
$\bar{K}_1^-$	A: s_2, z_2, $(3z^2-r^2)_2$
	B: $(1/2\sqrt{2})(x_1+\sqrt{3}\,y_1-\sqrt{3}\,x_2+y_2)$, $(1/2\sqrt{2})(xz_1+\sqrt{3}\,yz_1-\sqrt{3}\,xz_2+yz_2)$, $(1/2\sqrt{2})[xy_1+\sqrt{3}\,(x^2-y^2)_1-\sqrt{3}\,xy_2+(x^2-y^2)_2]$
	C: $(1/2\sqrt{2})(x_1+\sqrt{3}\,y_1+\sqrt{3}\,x_2-y_2)$, $(1/2\sqrt{2})(xz_1+\sqrt{3}\,yz_1+\sqrt{3}\,xz_2-yz_2)$, $(1/2\sqrt{2})[xy_1+\sqrt{3}\,(x^2-y^2)_1+\sqrt{3}\,xy_2-(x^2-y^2)_2]$
$\bar{K}_2^{(1)}$	A: x_2, y_1, xy_2, xz_2, yz_1, $(x^2-y^2)_1$
	B: $(\frac{1}{2}s_1-\frac{1}{2}\sqrt{3}\,s_2)$, $(\frac{1}{2}z_1-\frac{1}{2}\sqrt{3}\,z_2)$, $[\frac{1}{2}(3z^2-r^2)_1-\frac{1}{2}\sqrt{3}\,(3z^2-r^2)_2]$, $(1/2\sqrt{2})(\sqrt{3}\,x_1+y_1+x_2-\sqrt{3}\,y_2)$, $(1/2\sqrt{2})(\sqrt{3}\,xz_1+yz_1+xz_2-\sqrt{3}\,yz_2)$, $(1/2\sqrt{2})[\sqrt{3}\,xy_1+(x^2-y^2)_1+xy_2-\sqrt{3}\,(x^2-y^2)_2]$
	C: $(\frac{1}{2}s_1+\frac{1}{2}\sqrt{3}\,s_2)$, $(\frac{1}{2}z_1+\frac{1}{2}\sqrt{3}\,z_2)$, $[\frac{1}{2}\sqrt{3}\,(3z^2-r^2)_1+\frac{1}{2}(3z^2-r^2)_2]$, $(1/2\sqrt{2})(\sqrt{3}\,x_1+y_1-x_2+\sqrt{3}\,y_2)$, $(1/2\sqrt{2})(\sqrt{3}\,xz_1+yz_1-xz_2+\sqrt{3}\,yz_2)$, $(1/2\sqrt{2})[\sqrt{3}\,xy_1+(x^2-y^2)_1-xy_2+\sqrt{3}\,(x^2-y^2)_2]$
$\bar{K}_2^{(2)}$	A: x_1, y_2, xy_1, xz_1, yz_2, $(x^2-y^2)_2$
	B: $(\frac{1}{2}\sqrt{3}\,s_1+\frac{1}{2}s_2)$, $(\frac{1}{2}\sqrt{3}\,z_1+\frac{1}{2}z_2)$, $[\frac{1}{2}\sqrt{3}\,(3z^2-r^2)_1+\frac{1}{2}(3z^2-r^2)_2]$, $(1/2\sqrt{2})(x_1-\sqrt{3}\,y_1-\sqrt{3}\,x_2-y_2)$, $(1/2\sqrt{2})(xz_1-\sqrt{3}\,yz_1-\sqrt{3}\,xz_2-yz_2)$, $(1/2\sqrt{2})[xy_1-\sqrt{3}\,(x^2-y^2)_1-\sqrt{3}\,xy_2-(x^2-y^2)_2]$
	C: $(\frac{1}{2}\sqrt{3}\,s_1-\frac{1}{2}s_2)$, $(\frac{1}{2}\sqrt{3}\,z_1-\frac{1}{2}z_2)$, $[\frac{1}{2}\sqrt{3}\,(3z^2-r^2)_1-\frac{1}{2}(3z^2-r^2)_2]$, $(1/2\sqrt{2})(x_1-\sqrt{3}\,y_1+\sqrt{3}\,x_2+y_2)$, $(1/2\sqrt{2})(xz_1-\sqrt{3}\,yz_1+\sqrt{3}\,xz_2+yz_2)$, $(1/2\sqrt{2})[xy_1-\sqrt{3}\,(x^2-y^2)_1+\sqrt{3}\,xy_2+(x^2-y^2)_2]$
	$\bar{\Sigma}=(0,a)\quad 0<a<2\pi/\sqrt{3}$
$\bar{\Sigma}_1$	s_1, s_2, y_1, y_2, z_1, z_2, yz_1, yz_2, $(x^2-y^2)_1$, $(x^2-y^2)_2$, $(3z^2-r^2)_1$, $(3z^2-r^2)_2$
$\bar{\Sigma}_2$	x_1, x_2, xy_1, xy_2, xz_1, xz_2
	$\bar{T}=a(\frac{2}{3}\pi,2\pi/\sqrt{3})\quad 0<a<1$
$\bar{T}_1$	s_1, $(\frac{1}{2}\sqrt{3}x_1-\frac{1}{2}y_1)$, z_1, $[\frac{1}{2}\sqrt{3}xy_1-\frac{1}{2}(x^2-y^2)_1]$, $(\frac{1}{2}\sqrt{3}xz_1-\frac{1}{2}yz_1)$, $(3z^2-r^2)_1$, $(\frac{1}{2}x_2+\frac{1}{2}\sqrt{3}y_2)$, $[\frac{1}{2}xy_2+\frac{1}{2}\sqrt{3}\,(x^2-y^2)_2]$, $(\frac{1}{2}xz_2+\frac{1}{2}\sqrt{3}yz_2)$
$\bar{T}_2$	s_2, z_2, $(3z^2-r^2)_2$, $(\frac{1}{2}\sqrt{3}x_2-\frac{1}{2}y_2)$, $[\frac{1}{2}\sqrt{3}xy_2-\frac{1}{2}(x^2-y^2)_2]$, $(\frac{1}{2}\sqrt{3}xz_2-\frac{1}{2}yz_2)$, $(\frac{1}{2}x_1+\frac{1}{2}\sqrt{3}y_1)$, $[\frac{1}{2}xy_1+\frac{1}{2}\sqrt{3}\,(x^2-y^2)_1]$, $(\frac{1}{2}xz_1+\frac{1}{2}\sqrt{3}yz_1)$
$\bar{T}'$	$(x,2\pi/\sqrt{3})\quad 0<x<\frac{2}{3}\pi$
$\bar{T}_1'$	A: s_1, x_2, y_1, z_1, xy_2, xz_2, yz_1, $(x^2-y^2)_1$, $(3z^2-r^2)_1$,
	B: $(\frac{1}{2}s_1-\frac{1}{2}\sqrt{3}\,s_2)$, $(\frac{1}{2}y_1-\frac{1}{2}\sqrt{3}\,y_2)$, $(\frac{1}{2}z_1-\frac{1}{2}\sqrt{3}\,z_2)$, $(\frac{1}{2}yz_1-\frac{1}{2}\sqrt{3}\,yz_2)$, $[\frac{1}{2}(x^2-y^2)_1-\frac{1}{2}\sqrt{3}\,(x^2-y^2)_2]$, $[\frac{1}{2}(3z^2-r^2)_1-\frac{1}{2}\sqrt{3}\,z^2-r^2)_2]$, $(\frac{1}{2}\sqrt{3}x_1+\frac{1}{2}x_2)$, $(\frac{1}{2}\sqrt{3}xy_1+\frac{1}{2}xy_2)$, $(\frac{1}{2}\sqrt{3}xz_1+\frac{1}{2}xz_2)$
	C: $(\frac{1}{2}s_1+\frac{1}{2}\sqrt{3}\,s_2)$, $(\frac{1}{2}y_1+\frac{1}{2}\sqrt{3}\,y_2)$, $(\frac{1}{2}z_1+\frac{1}{2}\sqrt{3}\,z_2)$, $(\frac{1}{2}yz_1+\frac{1}{2}\sqrt{3}\,yz_2)$, $[\frac{1}{2}(x^2-y^2)_1+\frac{1}{2}\sqrt{3}\,(x^2-y^2)_2]$, $[\frac{1}{2}(3z^2-r^2)_1+\frac{1}{2}\sqrt{3}\,(3z^2-r^2)_2]$, $(\frac{1}{2}\sqrt{3}x_1-\frac{1}{2}x_2)$, $(\frac{1}{2}\sqrt{3}xy_1-\frac{1}{2}xy_2)$, $(\frac{1}{2}\sqrt{3}xz_1-\frac{1}{2}xz_2)$

TABLE I. *(Continued)*

Symmetry	Basis functions
$\bar{T}_2'$	A: s_2, x_1, y_2, z_2, xy_1, xz_1, yz_2, $(x^2-y^2)_2$, $(3z^2-r^2)_2$
	B: $(\frac{1}{2}\sqrt{3}\,s_1+\frac{1}{2}s_2)$, $(\frac{1}{2}\sqrt{3}\,y_1+\frac{1}{2}y_2)$, $(\frac{1}{2}\sqrt{3}\,z_1+\frac{1}{2}z_2)$, $(\frac{1}{2}\sqrt{3}yz_1+\frac{1}{2}yz_2)$, $[\frac{1}{2}\sqrt{3}\,(x^2-y^2)_1+\frac{1}{2}(x^2-y^2)_2]$, $(\frac{1}{2}\sqrt{3}\,(3z^2-r^2)_1+\frac{1}{2}(3z^2-r^2)_2]$, $(\frac{1}{2}x_1-\frac{1}{2}\sqrt{3}x_2)$, $(\frac{1}{2}xy_1-\frac{1}{2}\sqrt{3}xy_2)$, $(\frac{1}{2}xz_1-\frac{1}{2}\sqrt{3}xz_2)$
	C: $(\frac{1}{2}\sqrt{3}\,s_1-\frac{1}{2}s_2)$, $(\frac{1}{2}\sqrt{3}\,y_1-\frac{1}{2}y_2)$, $(\frac{1}{2}\sqrt{3}\,z_1-\frac{1}{2}z_2)$, $(\frac{1}{2}\sqrt{3}yz_1-\frac{1}{2}yz_2)$, $[\frac{1}{2}\sqrt{3}\,(x^2-y^2)_1-\frac{1}{2}(x^2-y^2)_2]$, $[\frac{1}{2}\sqrt{3}\,(3z^2-r^2)_1-\frac{1}{2}(3z^2-r^2)_2]$, $(\frac{1}{2}x_1+\frac{1}{2}\sqrt{3}x_2)$, $(\frac{1}{2}xy_1+\frac{1}{2}\sqrt{3}xy_2)$, $(\frac{1}{2}xz_1+\frac{1}{2}\sqrt{3}xz_2)$

and eighteenth layers had deficits of −0.27 and −0.11, respectively. With a lesser shift of −0.014 Ry on the surface to make the surface layer charge neutral, the nineteenth and eighteenth layers still were short −0.23 and −0.13 electrons/atom, while the thirteenth through seventeenth layer had surpluses of up to 0.05 electrons/atom. To smooth out this charge distribution, we shifted the three groups of (ss_0, pp_0, dd_0) parameters on the eighteenth, nineteenth, and surface (twentieth) layers by −0.007, −0.015, and −0.017 Ry, respectively, to produce planar charge densities of (starting from the surface plane and moving inward) 7.947, 8.009, 7.977, 7.998, 7.982, 8.033, 8.039, 8.000 electrons/atom with a deviation of less than 0.006 from the bulk value of 8.00 electrons/atom on the remaining planes. The deficit of 0.053 on the surface layer could have been removed by another iteration with slightly changed parameter shifts but it was not thought worthwhile since the shift of parameters on the first three planes would not affect the surpluses of 0.033 and 0.039 on the fifth and sixth planes in from the surface. A surplus of 0.042 electrons/atom was found on the third plane in from the (100) surface.[1] Since the parameter shifts there were confined to the surface plane and since the (100) interplanar separation is $\sqrt{3}$ times the (111), the surpluses in the two cases are about the same distance from the surface perturbation. Our surface charge of 7.947 electrons/atom had spin polarization 5.104↑ and 2.843↓ compared with the bulk 5.160↑ and 2.840↓. Because our parameter shifts are limited to zeroth-neighbor parameters, it is obvious that these planar charge densities are only approximate and that self-consistent calculations are needed.

TABLE II. Compatibility relations.

$\bar{\Gamma}_1^+ \rightarrow \bar{\Sigma}_1, \bar{T}_1$
$\bar{\Gamma}_1^- \rightarrow \bar{\Sigma}_1, \bar{T}_2$
$\bar{\Gamma}_3^+ \rightarrow \bar{\Sigma}_1, \bar{\Sigma}_2, \bar{T}_1, \bar{T}_2$
$\bar{\Gamma}_3^- \rightarrow \bar{\Sigma}_1, \bar{\Sigma}_2, \bar{T}_1, \bar{T}_2$
$\bar{M}_1^+ \rightarrow \bar{\Sigma}_1, \bar{T}_1'$
$\bar{M}_1^- \rightarrow \bar{\Sigma}_1, \bar{T}_2'$
$\bar{M}_2^+ \rightarrow \bar{\Sigma}_2, \bar{T}_2'$
$\bar{M}_2^- \rightarrow \bar{\Sigma}_2, \bar{T}_1'$
$\bar{K}_1^+ \rightarrow \bar{T}_1', \bar{T}_1$
$\bar{K}_1^- \rightarrow \bar{T}_2', \bar{T}_2$
$\bar{K}_2 \rightarrow \bar{T}_1', \bar{T}_2', \bar{T}_1, \bar{T}_2$

These results do strongly suggest, however, that the surface potential on the (111) face of bcc Fe is quite different from the surface potential on the (100) and (110) faces. This is not unexpected considering the considerable structural differences of the (111) surface. The (111) interplanar spacing is by far the smallest being $\frac{1}{3}$ the bulk nearest neighbor distance, i.e., one of an atom's nearest neighbors lies three planes away, whereas for the (100) and (110) surfaces the nearest neighbors were never any further than one plane away. Thus the atoms in the eighteenth plane, having lost a nearest neighbor, feel the presence of the surface strongly. This accounts for the need to vary the zeroth-neighbor parameters in the eighteenth layer to obtain even approximate charge neutrality. Along with a small interplanar spacing goes a large intraplanar spacing; there are no first or second neighbors to an atom within its own plane. Since our matrix element parameters include only first- and second-neighbor interactions, our model has no direct interaction between atoms on the same plane. This may account for the large flow of charge out of the eighteenth and nineteenth planes when the surface plane's zeroth parameters were shifted without corresponding shifts in the eighteenth and nineteenth planes. We mention in passing that it is these structure differences which make the (111) face the only one upon which the

catalytic conversion of N_2 and H_2 into ammonia occurs.[7]

The TDS and PDS for various planes in the forty layer film are given by Figs. 1 and 2 for the majority- and minority-spin cases, respectively. In both cases, the TDS and PDS on the interior planes near the middle of film are similar to the results from the (100) and (110) faces and to the bulk density of states of Tawil and Callaway[3] from which the parameters were derived. The surface PDS (plane 20) for both spins have the expected smaller second moment compared to the TDS. They have, in each spin, three sharp peaks which, especially for the peak of highest energy, are sharper and more extreme than the peaks in the TDS. The peaks are caused by surface resonances which we will discuss in detail in Sec. II. The PDS does not closely resemble the TDS until four or five layers into the film particularly in Fig. 1, the majority case. This long settling length is due to the surface potential shifts and structure of the (111) face.

The PDS for the two most interior planes are nearly identical and what differences do exist may be within the noise level. Somewhat larger are the differences between the TDS and interior plane PDS obtained here and those obtained previously for the (100) and (110) films. These differences we believe exceed the noise level and are due both to the relative thinness of this (111) film which is only 60% as thick as the previous (100) and (110) films and to the shift of the atomic parameters over three layers rather than just the surface layer.

These results for the surface PDS are similar to the results of Desjonqueres and Cyrot-Lackmann.[8] This similarity was at first surprising since significant differences between their results and ours were seen on the (100) and (110) films. In these cases the differences were traceable to

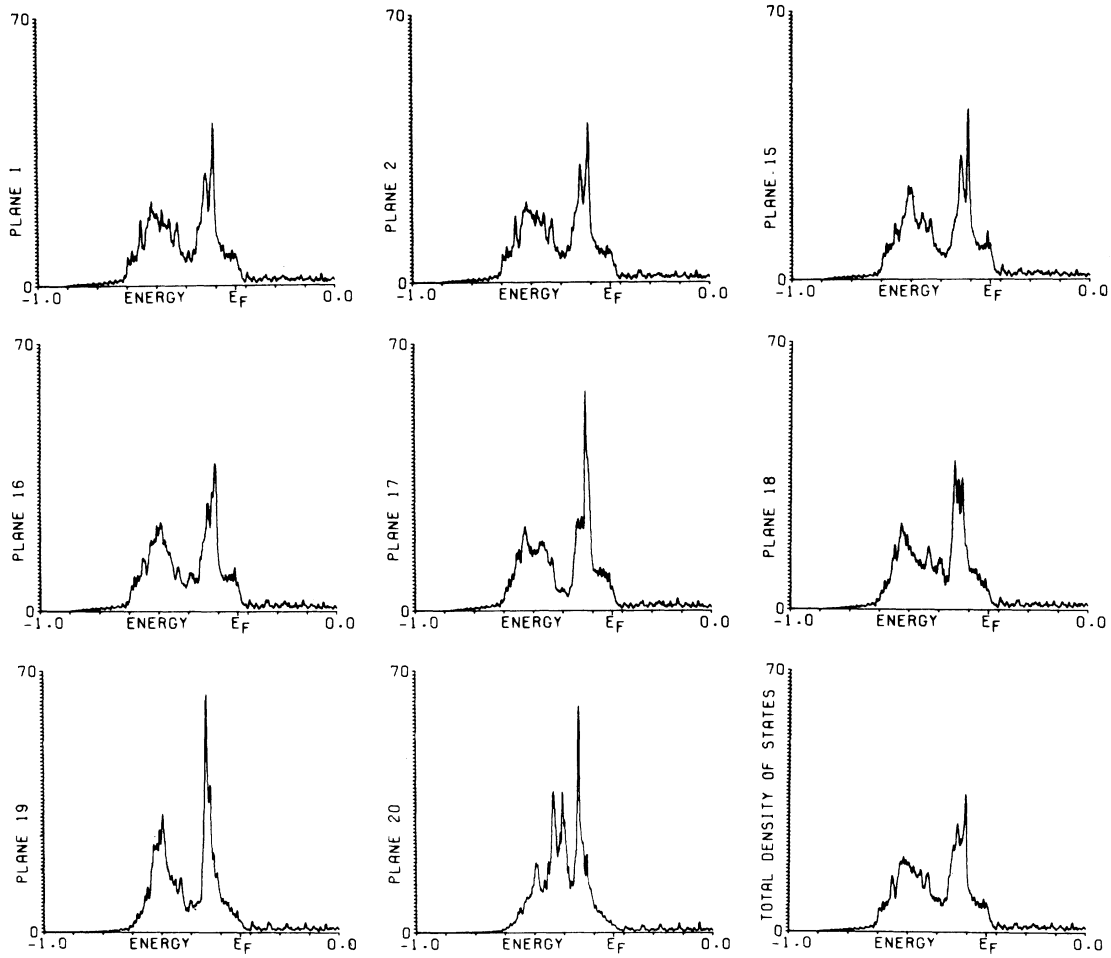

FIG. 1. Planar and total densities of states for the majority-spin case in units of electrons per atom per Ry. Layer 1 is the plane nearest the film center, while layer 20 is the surface plane.

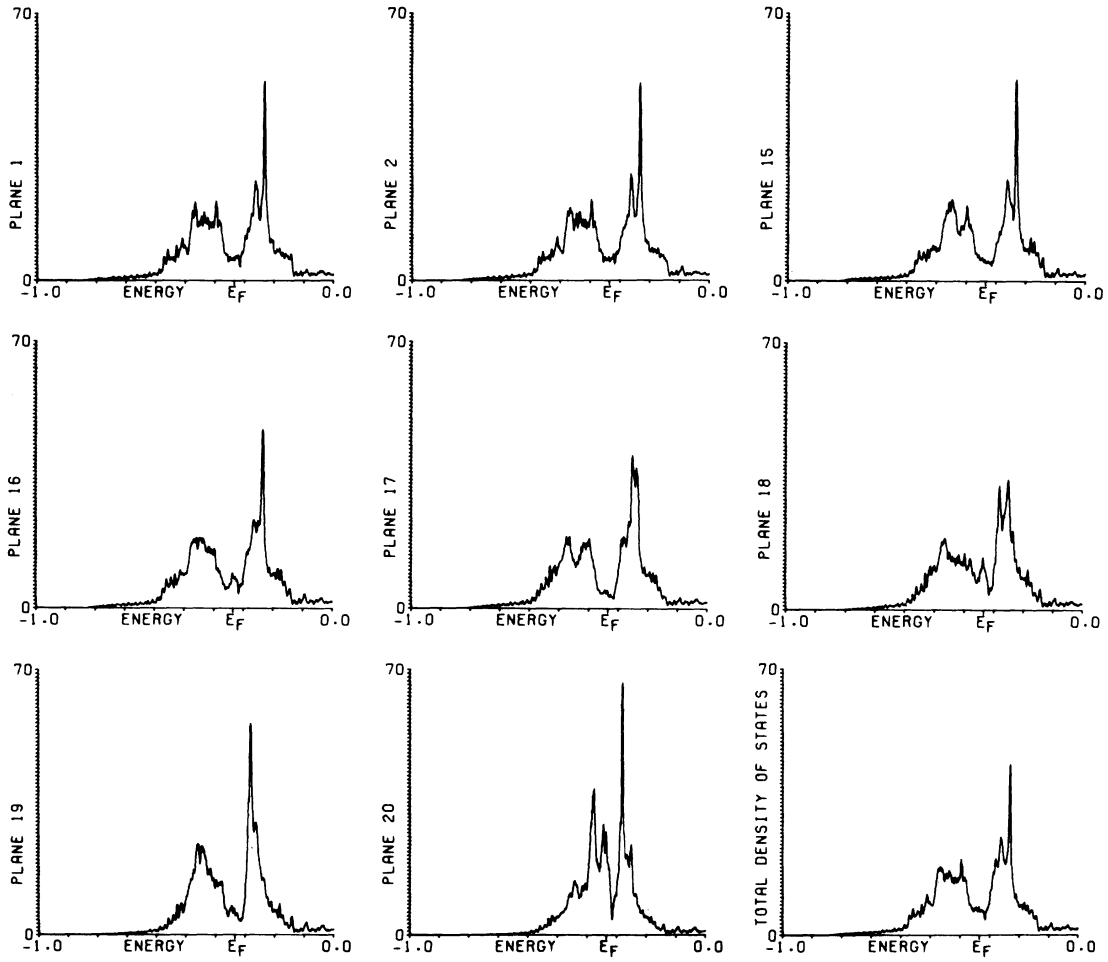

FIG. 2. Planar and total densities of states for the minority-spin case in units of electrons per atom per Ry. Layer 1 is the plane nearest the film center, while layer 20 is the surface plane.

the omission of s-d and p-d hybridization effects in their calculation. In Sec. II we will show that the structure seen in the surface PDS for this film is primarily due to d-band resonances rather than s-d or p-d hybridized surface states. Thus, the similarities in their and our results for the surface PDS are expected since their calculation does include an adequate d basis set. When we compare the potential shifts necessary to neutralize the surface charge in their calculation and ours, however, we find they required a larger shift for the (111) surface than required for their other surfaces, and their shift is, as for the other faces, opposite to ours, i.e., a repulsive shift. Since their tight-binding parameters are derived from a different calculation than Tawil and Callaway,[3] we do not know whether this discrepancy arises from calculation differences or characteristics of the bulk parameters.

Note added in manuscript. We now believe that the difference between their paramagnetic and our ferromagnetic calculation can be accounted for as follows. The paramagnetic Fermi energy lies on a large peak on the high-energy side of the TDS. The fact that the surface PDS is narrower than the TDS means that a large number of states above the Fermi energy in the TDS are below it in the surface PDS yielding a surplus of surface charge. In the ferromagnetic case the Fermi energy lies well above this peak in the majority-spin TDS so that the narrowing of the surface PDS causes only a very small majority-spin surface electron surplus. The Fermi energy lies in a minimum between the high- and low-energy peaks in the minority spin TDS. There is no *a priori* way to tell if the narrowing of the surface PDS will cause a net increase or decrease of minority spin states below E_F. The calculation of course shows that it

causes a moderately large deficit of minority-spin surface electrons which overwhelms the small majority-spin surplus. We believe that both this calculation and the paramagnetic[8] calculation underestimated the surface electronic charge (before the surface parameters were shifted) because the limited linear-combination-of-atomic-orbitals (LCAO) basis set could not account for the charge lying beyond the surface (which we consider to be part of the surface charge). One could try to correct this by putting atomic orbitals on the first missing plane of atoms. This, however, would be a poor basis set for describing the wave functions in a region where they have no atomic character. It furthermore would have the effect of adding 23 more unknown parameters to help fit the one known fact that the surface is charge neutral. We have just completed an *ab initio* supplemented-orthogonalized-plane-wave[9] calculation[10] for a 13-layer (100) paramagnetic iron thin film where we obtained a surface surplus of 1.5 electrons/atom which is considerably larger than that obtained from the LCAO calculation.[8,11] If we were to repeat this series of calculations on the three faces of iron, we would probably ignore surface charge neutrality altogether and choose unshifted surface parameters as giving a better picture of the energy bands in the ferromagnetic case. Fortunately, the hybridized surface states are fairly insensitive to the surface parameters. On the (111) face most of the surface states are unhybridized; however, the effect of the surface parameter shift was to pull some surface states into the gaps and other surface states out so that the total number of surface states was practically unchanged as was the overall picture of the energy bands.

II. STRUCTURE OF THE ENERGY BANDS

Figures 3–5 are the energy bands for this (111) 40-layer film of ferromagnetic iron. In each figure, the upper set of bands are for the minority spin while the lower set are the majority spin case. Figure 3 shows the composite band structure along the $\bar{\Sigma}$, $\bar{T}'$, and $\bar{T}$ directions. Figures 4 and 5 show the subbands $\Sigma_1, \bar{T}_1', \bar{T}_1$ and $\bar{\Sigma}_2, \bar{T}_2', \bar{T}_2$, respectively. Surface states, when the gaps containing them are visible, are indicated by solid lines for as long as the surface states persist. The bands at the high-symmetry points are also shown with pairs of surface states indicated by the dots. As was the case for the bands of the (100) and (110) films, the minority-spin bands, aside from an upward shift of about 0.07 Ry, are very similar to the majority-spin bands.

For the (100) and (110) films, surface states always occurred in pairs with one state in the "+" reflection symmetry and the other in the "−" reflection symmetry. The present case still has surface states occurring in pairs but the grouping depends on the location of the surface states in $\bar{k}$ space. For surface states at $\bar{M}$ and $\bar{\Gamma}$ one state occurs in the even and one in the odd inversion symmetries. In the $\bar{K}_1$ symmetries, one state will belong to $\bar{K}_1^+$ and one to $\bar{K}_1^-$. The $\bar{K}_2$ pair of surface states are partners in the two-fold degenerate $\bar{K}_2$ representation. This is the only case in which the pair of surface states remains degenerate even if the decay length is large compared to the film thickness. One can choose the $\bar{K}_2$ surface states to be either even and odd under the two-fold rotation about the $\bar{K}$ axis or to be localized on the film surfaces. Surface states in $\bar{T}_1'$ (or $\bar{T}_1$) will have one member of the pair in $\bar{T}_1'$ (or $\bar{T}_1$) with the other member in $\bar{T}_2'$ (or $\bar{T}_2$). Surface states occurring in $\bar{\Sigma}_1$, $\bar{\Sigma}_2$ or at a $\bar{k}$ of no symmetry occur as pairs within the same representation since the group of the wave vector contains no operation that interchanges the two surface planes.

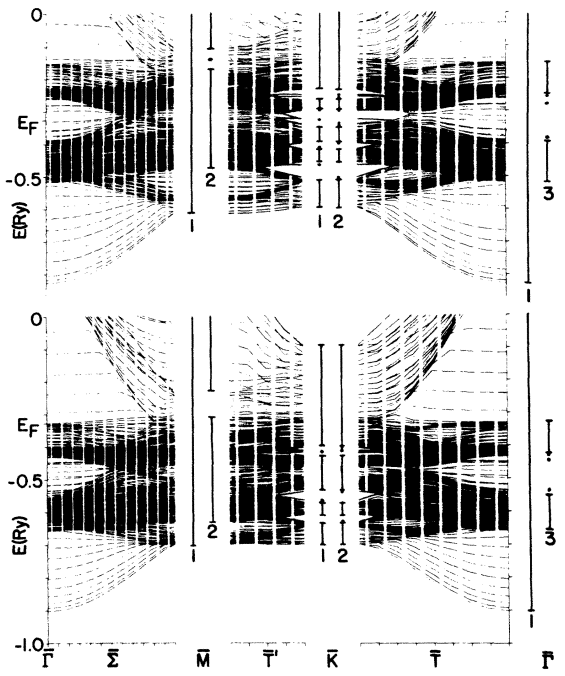

FIG. 3 Majority- and minority-spin energy bands. The upper set is the minority bands and the lower set the majority bands.

Beginning with the composite bands in Fig. 3, we find the only absolute gaps, for either spin, are located around the $\bar{K}$ point. The majority-spin bands have four gaps at $\bar{K}$ with the largest gap opening upward around $\bar{K}$ from −0.1 Ry. This gap does contain a surface state at +0.047 Ry which is not shown in the picture. The lower three $\bar{K}$ gaps

persist briefly in the $\bar{T}$ and $\bar{T}'$ directions and contain a total of six pairs of $\bar{K}_1$ and $\bar{K}_2$ surface states which, like the gaps, continue briefly in the $\bar{T}$ and $\bar{T}'$ directions. Although these states moved when the surface potentials were adjusted to obtain approximate charge neutrality, the total number of surface states in these gaps (and elsewhere in the film) remained constant. The minority composite bands and absolute gaps differ in only two points. The uppermost $\bar{K}$ gap has moved to above the vacuum level while an additional small gap has opened around $\bar{K}$ around the Fermi level. In the minority bands there are ten pairs of surface states at $\bar{K}$ and they persist, as in the majority bands, briefly in the $\bar{T}'$ and $\bar{T}$ directions.

The $\bar{\Sigma}_1$, $\bar{T}_1'$, and $\bar{T}_1$ bands of Fig. 4 show no new band gaps or surface states. In the $\bar{\Sigma}_1$ bands near $\bar{M}$ at -0.5 Ry for the majority and -0.3 Ry for the minority bands, the band structure seems to indicate a gap containing a single $\bar{\Sigma}_1$ surface state. This apparent but actually non-existent gap is the result of our finite 40-layer film where a rapidly rising s band covers a gap between two very dense d bands. The apparent surface state is one of what would be a continuum of s-band bulk states in a semi-infinite crystal.

The $\bar{\Sigma}_2$ bands in Fig. 5 contain, for each spin, two subband gaps which exist only in the $\bar{\Sigma}_2$ states and do not persist in any direction away from $\bar{\Sigma}$.

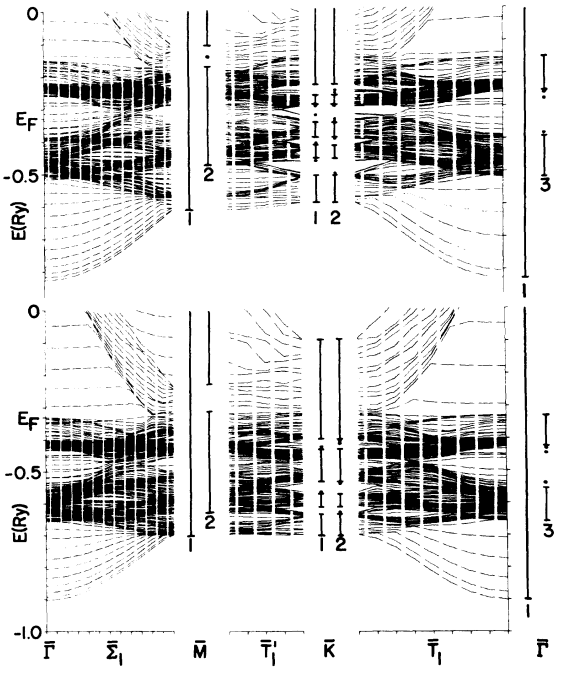

FIG. 4. Majority- and minority-spin energy bands for the $\bar{\Sigma}_1$, $\bar{T}_1'$, and $\bar{T}_1$ symmetries. The upper set is the minority bands and the lower set the majority bands.

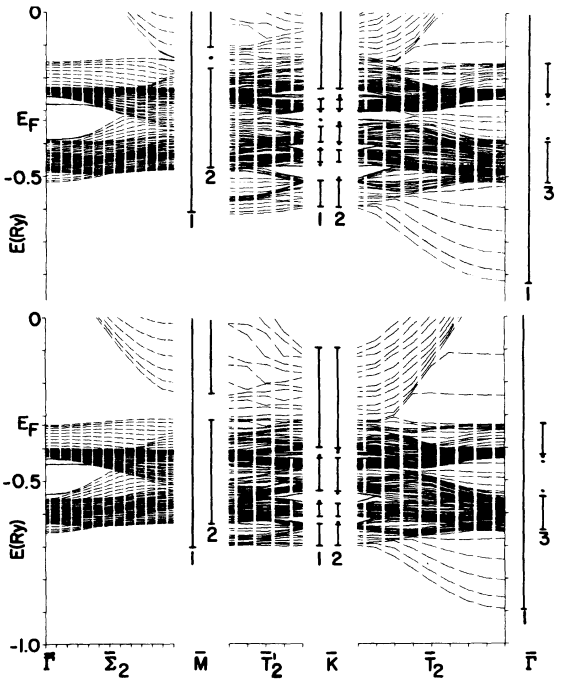

FIG. 5. Majority- and minority-spin energy bands for the $\bar{\Sigma}_2$, $\bar{T}_2'$, and $\bar{T}_2$ symmetries. The upper set is the minority bands and the low set the majority bands.

The upper gap at $\bar{\Gamma}$ runs from the top of the upper $\bar{\Gamma}_3$ band to well above the vacuum level. It narrows down as it approaches $\bar{M}$ where it coincides with the $\bar{M}_2$ gap. This gap in the majority bands does not contain any surface states. The second gap opens at $\bar{\Gamma}$ as a $\bar{\Gamma}_3$ gap around -0.5 Ry and pinches off midway to $\bar{M}$. It contains three $\bar{\Sigma}_2$ pairs of surface states along the top, upper middle, and bottom of the gap. These states persist as resonances away from $\bar{\Sigma}$. Since $\bar{\Gamma}_3^+$ and $\bar{\Gamma}_3^-$ are themselves two-fold degenerate, the $\bar{\Sigma}_1$ bands contain resonances near $\bar{\Gamma}$ which account for the other six surface states indicated at $\bar{\Gamma}_3$. For the minority $\bar{\Sigma}_2$ bands, the lower gap, now centered around the Fermi energy, is similar to its majority spin counterpart. The upper $\bar{\Sigma}_2$ gap near $\bar{M}$ has a surface state pair going into $\bar{M}_2$ which is identifiable only near $\bar{M}$. These surface states have very long decay lengths, requiring some 15 layers to decay to $1/e$ of their surface amplitude. The band limits and the decay length of the surface states at $\bar{M}_2$ were determined by a calculation on a 120-layer film. These surface states are nearly independent of the surface potential and arise from the same kind of bulk band structure as caused identical $\bar{M}_5$ surface states in the (100) face calculation. In the (100) case the gap pinched off where the surface states disappeared and then reopened. Because

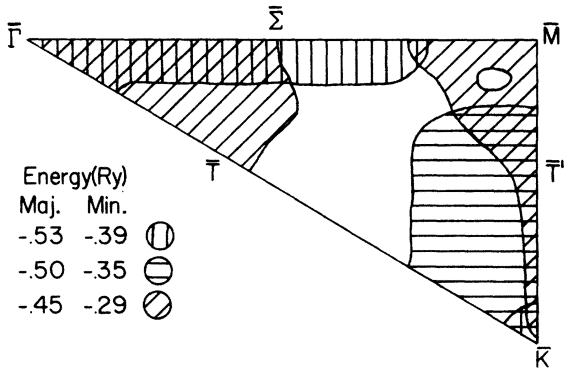

FIG. 6. Extent of the significant resonances in the 2D BZ. Although the energies of the resonance bands are different for the two spin cases, the number of these bands and their extents in the 2D BZ were found to be the same. The cross-hatched regions indicate where the resonances are most pronounced.

of the lower symmetry, we have not checked to see if that is the case here although we believe it is.

Because these surface states are so few and cover such small regions of $\bar{k}$ space, they do not significantly contribute to the PDS on the surface and near surface planes. Resonances, on the other hand, account for almost all of the structure seen in the surfaces PDS for both the majority and minority spin bands. Because the d bands are so flat, and since there are no major gaps to bend the paths of these resonances, the resonances in both spins run around the 2D BZ in very flat bands and produce sharp peaks in the surface PDS shown in Figs. 1 and 2. Figure 6 shows the regions of the $\frac{1}{12}$ 2D BZ over which these resonances are most prevalent. Note, for each spin, there are three resonance bands and that the minority resonances cover the same areas as their majority-spin counterparts but occur in an energy approximately 0.15 Ry higher. This shift is somewhat greater than the shift of 0.07 Ry seen at the bottom of the bands but instead corresponds to the approximate displacement of the d bands between the two spins. This displacement is best seen in Fig. 5 in the pure $d\bar{\Sigma}_2$ bands. Note that the high-energy peak in the density of states (Figs. 1 and 2) is a double peak whose high-energy side is larger in the interior but that as the surface is approached, the high-energy side is quenched and the low-energy side becomes the largest peak in the PDS. This peak is due to the highest-energy resonance and the eigenfunctions of this resonance tend to have large amplitude on both the surface and first interior plane. Indeed, for the minority spins this PDS peak is somewhat larger on the nineteenth plane than on the twentieth. The medium-energy resonance wave functions are large only on the surface plane and this peak appears only on the surface PDS. The low-energy resonance wave functions tend to have large amplitude as far as two or three layers below the surface. This resonance is visible as a peak, however, only on the surface PDS. It contributes to the upper shoulder of the broad low-energy PDS peak for several layers below the surface.

---

*Supported by NSF Grant No. DMR 73-02449-A02.

[1]D. G. Dempsey, L. Kleinman, and E. Caruthers, Phys. Rev. B 12, 2932 (1975).

[2]D. G. Dempsey, L. Kleinman, and E. Caruthers, Phys. Rev. B 13, 1489 (1976).

[3]R. A. Tawil and J. Callaway, Phys. Rev. B 7, 4242 (1973).

[4]E. B. Caruthers, L. Kleinman, and G.P. Alldredge, Phys. Rev. B 9, 3330 (1974).

[5]These 61 points are given by $\bar{k} = \frac{1}{24}(m\vec{K}_1 + n\vec{K}_2)$ with the three conditions $m + \frac{1}{2}n \leq 12$, $m + n \leq 16$, $m \geq n$ and where m and n are zero or positive integers and $\vec{K}_1 = (2\pi/a)(-\frac{1}{3}, -\frac{1}{3}, \frac{2}{3})$ and $\vec{K}_2 = (2\pi/a)(\frac{2}{3}, -\frac{1}{3}, -\frac{1}{3})$.

[6]See Ref. 12 of Ref. 2.

[7]R. Brill, E. L. Richter, and E. Ruch, Angew. Chem. Internat. Edit. 6, 882 (1967).

[8]M. C. Desjonqueres and F. Cyrot-Lackman, J. Phys. F 5, 1368 (1975).

[9]L. Kleinman and E. Caruthers, Phys. Rev. B 10, 3213 (1974).

[10]E. Caruthers, D. G. Dempsey, and L. Kleinman, following paper, Phys. Rev. B 14, 288 (1976).

[11]The surface charge surplus is not given in Ref. 8. However, from the surface PDS curve and the surface parameter shift, we estimate it to be about $\frac{1}{2}$ electron/atom.